Biomaterials 32 (2011) 1477–1483

Contents lists available at ScienceDirect

Biomaterials

journal homepage: www.elsevier.com/locate/biomaterials

High-throughput generation of hydrogel microbeads with varying elasticity for cell encapsulation

Alexander Kumachev [a], Jesse Greener [a], Ethan Tumarkin [a], Erika Eiser [b], Peter W. Zandstra [c,d], Eugenia Kumacheva [a,c,d,*]

[a] Department of Chemistry, University of Toronto, 80 Saint George Street, Toronto, Ontario M5S 3H6, Canada
[b] Cavendish Laboratory, University of Cambridge, JJ Thomson Avenue, Cambridge CB3 0HE, United Kingdom
[c] Institute of Biomaterials & Biomedical Engineering, University of Toronto, 164 College Street, Toronto, Ontario M5S 3G9, Canada
[d] Department of Chemical Engineering and Applied Chemistry, University of Toronto, 200 College Street, Toronto, Ontario M5S 3E5, Canada

ARTICLE INFO

Article history:
Received 30 September 2010
Accepted 15 October 2010
Available online 20 November 2010

Keywords:
Hydrogel
Microfluidics
Microencapsulation
Mechanical properties
Stem cell

ABSTRACT

Elasticity of cellular microenvironments strongly influences cell motility, phagocytosis, growth and differentiation. Currently, the relationship between the cell behaviour and matrix stiffness is being studied for cells seeded on planar substrates, however in three-dimensional (3D) microenvironments cells may experience mechanical signalling that is distinct from that on a two-dimensional matrix. We report a microfluidic approach for high-throughput generation of 3D microenvironments with different elasticity for studies of cell fate. The generation of agarose microgels with different elastic moduli was achieved by (i) introducing into a microfluidic droplet generator two streams of agarose solutions, one with a high concentration of agarose and the other one with a low concentration of agarose, at varying relative volumetric flow rate ratios of the two streams, and (ii) on-chip gelation of the precursor droplets. At 37 °C, the method enabled a ~35-fold variation of the shear elastic modulus of the agarose gels. The application of the method was demonstrated by encapsulating two mouse embryonic stem cell lines within the agarose microgels. This work establishes a foundation for the high-throughput generation of combinatorial microenvironments with different mechanical properties for cell studies.

Cellular microenvironments have a broad range of mechanical properties. For example, brain, muscle, osteoid matrix and bone tissues have elastic moduli of 0.1–1, 8–17, 25–40 and ~1.5×10^7 kPa, respectively [1–3]. Cells have developed mechanisms to sense the stiffness of the surrounding matrix by adhering to and pulling upon it, followed by a cytoskeletal cellular response [4]. Matrix stiffness influences many aspects of cell behaviour, e.g., cell motility [5], phagocytosis [6], and differentiation [7]. In particular, recent studies of the relationship between the stiffness of the substrate and the lineage specification of stem cells suggested the need for optimizing the mechanical properties of cellular microenvironments for regenerative applications using progenitor cells. For example, when naïve mesenchymal stem cells were seeded under identical serum conditions onto collagen-coated polyacrylamide gels with various elasticities, the cells specified their lineage towards neurons, myoblasts, and osteoblasts on matrices with low, intermediate and high elastic moduli, respectively [8]. In other studies, matrix stiffness affected cell adhesion [9], and the formation of myofibroblasts from interstitial cells [10].

Currently, most of the research on the relationship between matrix stiffness and cell behaviour is being conducted for cells seeded on planar substrates, yet, a majority of tissue cells are exposed to three-dimensional (3D) environments, that is, they are surrounded by a complex set of extracellular matrix (ECM) proteins. Matrix forces transmitted to cells in 3D environments are generally different than on planar surfaces. Cell–ECM interactions provide biochemical and mechanical cues that directly affect cell function [11]. Encapsulation of cells within hydrogel materials with different elasticity enables the investigation of the role of the mechanical properties of 3D environments on cell behaviour. Synthetic and natural hydrogel matrices have been used for cell culture, as well as for tissue-specific differentiation of stem cells [12–15]. Among these studies, the microbead format for cell culture allows the localization of cells within a small amount of a physiologically relevant matrix – a microenvironment – and an easy exchange of nutrients and gases between the encapsulated cells and the surrounding medium [16,17]. The preparation of microbeads with

* Corresponding author. Department of Chemical Engineering and Applied Chemistry, University of Toronto, 200 College Street, Toronto, Ontario M5S 3E5, Canada. Fax: +1 416 978 3576.
E-mail address: ekumache@chem.utoronto.ca (E. Kumacheva).

0142-9612/$ – see front matter
doi:10.1016/j.biomaterials.2010.10.033

varying mechanical properties to study the effect of varying matrix composition on cell fate, e.g., cell viability, morphology, or differentiation is yet to be reported.

Recently, microfluidics (MFs) heralded new opportunities for fundamental studies in cell biology [18]. In particular, MFs has been used for the generation of well-defined cellular microenvironments by encapsulating cells in droplets or microgels, followed by studies of cell growth and viability [19–21], gene expression [22,23], and enzymatic activity [24–26]. The MF encapsulation strategy offered several important advantages: the ability to create 3D cellular microenvironments (niches) with precisely controlled dimensions and chemical and mechanical properties; the capability to vary the properties of these environments in a high-throughput, combinatorial manner; and a high frequency – on the order of 10^2 to 10^3 s^{-1} – of the generation of cellular microenvironments that can be used as massive combinatorial libraries.

The primary objective of the current study was to develop a method for the high-throughput generation of hydrogel agarose microbeads (microgels) with varying mechanical properties, which are to be used for the encapsulation of cells and subsequent studies of the effect of matrix elasticity on cell fate. Agarose is a neutral polysaccharide that forms hydrogels at reduced temperatures [27]. It is extensively used in biomedical research, in particular, in cell culture systems, owing to the following useful properties: it is generally bio-inert, it is non-adsorptive to proteins and non-adhesive to cells, it can be readily functionalized with cell adhesion or other signalling molecules and its mechanical properties can be tuned by varying the agarose concentration in the gel [28–31]. In our work, agarose microgels with precisely controlled dimensions and tuneable elasticity were produced by MF emulsification of solutions with varying agarose concentration and subsequent fast gelation of droplets.

1. Materials and methods

1.1. Materials

Agarose with a gelling temperature in the range of 18–26 °C (ultra-low gelling temperature agarose) was purchased from SeaPrep (Lonza, Switzerland, www.lonza.com). Phosphate buffer solution (1 wt.%) was purchased from Gibco-BRL (Rockville, MD). A non-ionic surfactant Span-80, mineral oil and glycerol were supplied by Aldridge-Sigma Canada. A 3 wt.% agarose solution was prepared by dissolving 1.5 g of agarose in 48.5 g of a 1 wt.% PBS solution under heating to 70 °C, and subsequent cooling to room temperature. Agarose solutions with a concentration of 0.5 wt.% were prepared by dilution of the stock solution with a 1 wt.% PBS buffer solution. A non-ionic surfactant Span-80 was dissolved to a concentration of 3 wt.% in mineral oil with a viscosity of 30 cPs (Gelest Inc., www.gelest.com).

1.2. Methods

1.2.1. Fabrication of MF devices

Photolithographic masters were prepared from SU-8 25 photoresist (MicroChem) in bas-relief on silicon wafers. The MF devices were fabricated in poly (dimethylsiloxane) (Sylgard 184, Dow Corning) using a standard soft lithography method [32]. Prior to the preparation of cell-free agarose microgels, the MF device was maintained for 48 h in an oven at 140 °C.

For cell encapsulation experiments, the sealed MF device was maintained for 12 h in an oven at 140 °C and subsequently exposed to the vapour of 1,1,1,3,3,3-hexamethyldisilazane (99.9% pure, Sigma, U.S.A.). During silanization, the MF devices were placed on a hot plate at 80 °C for 1 h. The silanizing agent was placed into a 25 mL vial sealed with a sleeve style rubber stopper (Wheaton Science Products, U.S.A.). A N_2 gas was bubbled through the silanizing agent. The vapour of 1,1,1,3,3,3-hexamethyldisilazane was supplied to the MF device via polyethylene tubing (Small Parts, U.S.A.). Prior to cell encapsulation, the MF device was extensively washed with 70 vol.% ethanol/water mixture and then with double distilled water.

1.2.2. Characterization of the composition of emulsified agarose solutions

The composition of the emulsified agarose solutions (and the corresponding agarose microgels) was determined by on-chip Attenuated Total Reflection Fourier Transform Infrared Spectroscopy (ATR-FTIR) [33]. A single reflection diamond ATR crystal (PIKE Tech.) was interfaced with the microchannel where mixing of the two streams of agarose solutions took place. Absorbance measurements of the absorption band for the C–O–C vibration of agarose $\nu_{C-O-C} = 1070$ cm^{-1} were acquired using a Vertex 70 FTIR spectrometer (Bruker Inc.). Opus 6.5 software was used for data acquisition, manipulation and analysis. A calibration curve was generated by measuring the intensity of the ν_{C-O-C} peaks for the agarose solutions with known concentrations. The absorbance, A, changed linearly with concentration, following the Beer–Lambert relation,

$$A = C_{ag} \times l \times \varepsilon \quad (1)$$

where C_{ag} is the agarose concentration in the solution, l is the penetration depth of the evanescent IR light and ϵ is the extinction coefficient. The experimental details of ATR-FTIR experiments are provided in Supporting Information.

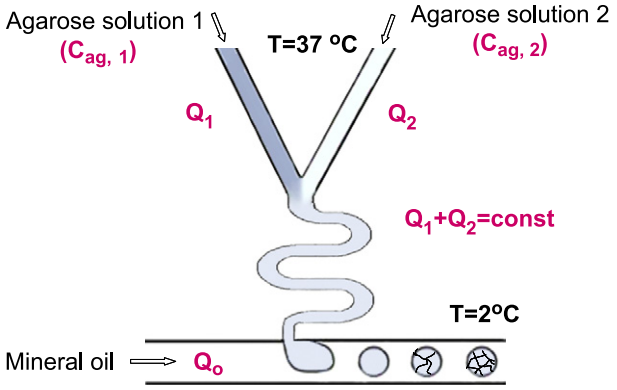

Fig. 1. Schematic of the MF device for the generation of agarose microgels with tunable elasticity. The height of the device was 150 μm. The width of the horizontal channel supplying the mineral oil phase and the width of the serpentine channel at the point of T-junction were was 150 and 20 μm, respectively. The length of the mixing channel was 250 mm.

1.2.3. Characterization of the rheological properties of agarose solutions and gels

The temperature-dependent viscosity of agarose solutions with various concentrations of agarose was determined in a stress-controlled rheometer (Physica MCR501, Anton Paar). A thermostated cap was used to avoid temperature gradients during measurements. In viscosity measurements, the cone-plate geometry (a diameter of 50 mm) contained a gap sensor that maintained a constant gap of 50 μm between cone and plate throughout the temperature window of 5–60 °C. After loading the agarose solutions at 60 °C, the viscosity measurements were conducted in the Newtonian regime by applying a constant shear rate of 10 s^{-1}, while cooling the sample with a rate of ~1 °C/min until 4 °C was reached. After each measurement, the sample was replaced with a fresh one, in order to avoid the effect of drying. In the present work we present the values of viscosity measured at 32 °C (the temperature of emulsification).

The elastic shear modulus, G', of macroscopic agarose gels with different concentrations of agarose was measured by using frequency sweeps in the plate–plate geometry. An agarose solution was loaded in the instrument and gelled by cooling it to 4 °C. Then, a strain with amplitude of 1 Pa was applied by varying the angular frequency from 0.1 to 50 Hz. Control experiments were carried out by using lower stress amplitudes and also by applying a strain amplitude of 1%, verifying that the measurements captured the viscoelastic response of the gels in the linear regime by varying the angular frequency from 0.1 to 50 Hz. In the present work we report the values of G' that were determined at the angular frequency of 0.1 Hz after incubating gels with varying agarose concentrations for 10–15 min at temperatures of 4, 25 and 37 °C.

1.2.4. Generation of agarose microgels

Agarose microgels with varying mechanical properties were produced by the MF emulsification of solutions with varying agarose concentration and subsequent gelation of the precursor droplets by thermosetting. The MF device contained a T-junction droplet generator followed by a straight downstream channel where gelation took place (Fig. 1). Two agarose solutions with concentrations of 3.0 and 0.5 wt.% were supplied to the two inlets of the MF device using two independently controlled syringe pumps (Harvard Apparatus 33 Dual Syringe Pump, U.S.A.). Later in the text we refer to the solutions with agarose concentration of 3.0 and 0.5 wt.% as to Streams 1 and 2, respectively. Both solutions were heated to 37 °C by placing the syringe pumps in an oven, however at the point of emulsification their temperature was reduced to 32 ± 1.0 °C (verified by measuring the temperature with a thermocouple). The total flow rate of Streams 1 and 2 was $Q_d = 0.12$ mL/h. The solutions were mixed in a serpentine channel with the length of 250 mm (Fig. 1). Thorough mixing of the solution in the wavy channel was verified by introducing a blue food dye in Stream 1 and monitoring the distribution of the dye in the mixed solution

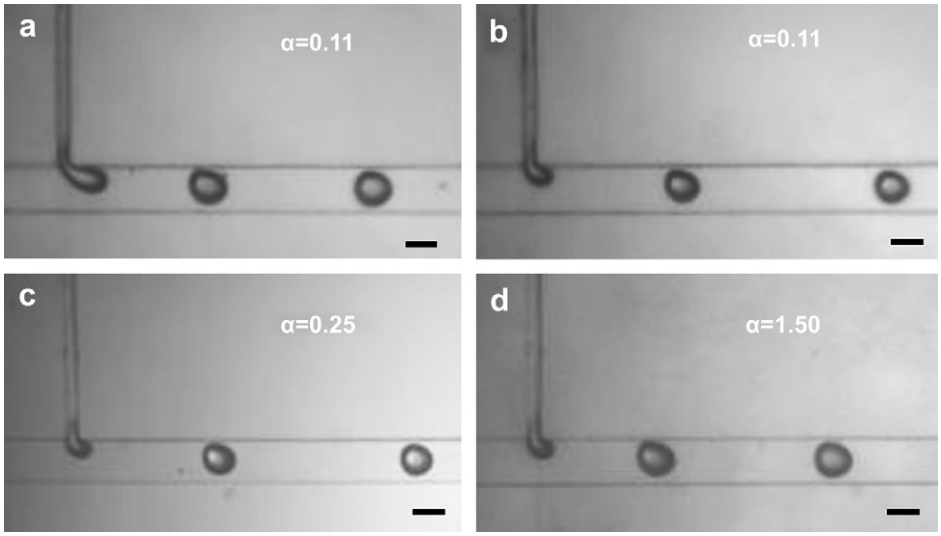

Fig. 2. Optical microscopy images of agarose droplets forming at a T-junction of the MF device. The images of droplets in (a) and (b) were taken at Q_o of 0.4 and 0.6 mL/h, respectively, at $\alpha = 0.11$. The images of droplets (c) and (d) were taken at $Q_o = 0.9$ mL/h at α of 0.25 and 1.50, respectively. $Q_d = 0.12$ mL/h. The scale bar is 100 μm.

along the mixing channel. The concentration of agarose in the droplets was varied by tuning the ratio between the volumetric flow rates of the Streams 1 and 2. At the T-junction, the stream of the mixed agarose solution broke up and released droplets of the mixed agarose solution.

The droplets travelled 250 mm in the downstream channel towards the outlet of the MF device and then exited into an outlet tubing (HPFA tubing, Upchurch Scientific, U.S.A.). The outlet tubing was enclosed by a hose connected to a water circulator cooled to 2 °C by a 1:4 vol. mixture glycerol and water. The droplets moved through the cooled tubing for approximately 5 min and were collected in a 15 mL conical tube filled with PBS solution. The tube was placed in an ice bath for 45 min to ensure complete gelation of the microgels. The resulting suspension was centrifuged at 1000 rpm at 4 °C for 5 min, washed with a PBS buffer, and transferred into a PBS buffer.

1.2.5. Cell encapsulation

Two murine embryonic stem (mES) cell lines were used in the present work: R1 mES cells labelled with Vybrant Cell Tracer carboxyfluorescein diacetate succinimidyl ester (CFDA SE "green" (Invitrogen)) and YC5–YFP–NEO mES cells transfected to produce yellow fluorescent protein [34]. Each cell suspension was prepared to a concentration of 8×10^6 cells/mL in agarose solutions in an HBSS (Gibco-BRL, Rockville, MD) buffer pre-heated to 37 °C. Two suspensions containing an equal concentration of cells were supplied to two channels of the MF device, as shown in Fig. 1. Following the gelation of the precursor droplets, microgels were centrifuged at 1000 rpm at 4 °C for 5 min, washed twice with HBSS buffer, and transferred into cell culture media.

1.2.6. Cell culture

Cells were cultured under sterile conditions and maintained in a 5% CO_2 humidified incubator at 37 °C. Microgels laden with R1 or YC5–YFP–NEO mES cells were maintained in cell culture media composed of Dulbecco's Modified Eagle Media (DMEM, Gibco-BRL) supplemented with 15% (v/v) Fetal bovine serum (FBS, Gibco-BRL), 2 mM L-glutamine, 0.1 mM beta-mercaptoethanol (BME, Sigma, St. Louise, MO), 0.1 mM non-essential amino acids (NEAA, Gibco-BRL), 1 mM sodium pyruvate (Gibco-BRL), 50 μg/mL penicillin (Gibco-BRL), 50 μg/mL streptomycin (Gibco-BRL), and 500 pM Leukemia inhibitory factor (LIF, Chemicon, Temecula, CA). Confluent dishes of mES cells were fed and passaged on alternate days. Fluorescence microscopy images of encapsulated cells were captured using a Zeiss Microscope (Axio Observer D1, U.S.A.) coupled with a digital camera (Axio Cam HRm, Zeiss, U.S.A.).

2. Results and discussion

To develop a method for MF generation of libraries of hydrogel microenvironments with different mechanical properties for cell studies we used the following considerations.

(i) The concentrations of agarose in the concentrated and dilute solutions (supplied as Streams 1 and 2, respectively) had to be such that sufficient mixing occurred in the serpentine channel and controlled emulsification took place in the MF droplet generator with a geometry shown in Fig. 1;
(ii) The lower limit of C_{ag} in the precursor droplets was determined by the integrity of the corresponding microgels in HBSS solution at 37 °C, that is, under cell culture conditions;
(iii) Microgels derived from solutions with varying C_{ag} had to have identical average dimensions;
(iv) To avoid the potential impact of droplet coalescence on broadening the distribution of sizes of microgels, it was important to achieve sufficient pre-gelation of droplets in the downstream channel of the MF device (complete droplet gelation was carried out *off-chip*);
(v) To achieve a 100% cell encapsulation efficiency, we used the Poisson distribution equation as in [35]

$$P(x,\lambda) = \frac{e^{-\lambda}\lambda^x}{x!} \quad (2)$$

where $P(x,\lambda)$ is the fraction of microgels containing x cells, and λ an average number of cells per microgel. For the concentration of cells in the droplet phase of 8×10^6 cell/mL, we estimated that a 100% encapsulation efficiency would be achieved by generating droplets with a diameter of 110 μm.

In the experiments, we denoted the ratio of volumetric flow rates of Stream 1-to-Stream 2 as α. The value of α was tuned from 0.11 to 9.0. Fig. 2a–d shows typical optical microscopy images of the droplets formed from the agarose solution at various values of α. The droplets formed in the pinching regime without obstruction of the downstream channel, due to the shear stress imposed by the oil phase [36]. The dimensions of droplets were tuned to be in the range from 125 to 100 μm by varying the flow rate of the continuous oil phase. The frequency of droplet generation was approximately 40 s^{-1}. The effect of the flow rate of the continuous phase, Q_o, on the droplet dimensions is illustrated in Fig. 2a and b. At $\alpha = 0.11$, increasing the value of Q_o resulted in smaller droplet sizes. More importantly, for a particular value of Q_o, the size of droplets became smaller with decreasing values of α. For example, at $Q_o = 0.9$ mL/h the average diameters of droplets were 104 and 117 μm for $\alpha = 0.25$ and $\alpha = 1.50$ (Fig. 2c and d, respectively).

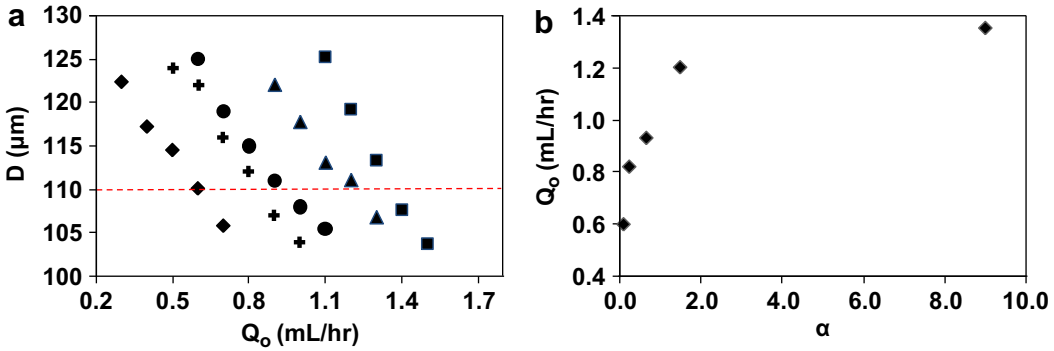

Fig. 3. (a) Variation in droplet diameter, D, plotted as a function of the flow rate of the continuous phase, Q_o, for α of 0.11 (◆), 0.25 (+), 0.67 (•), 1.50 (▲), and 9.00 (■). For each experimental point we analyzed 100 droplets generated in three independent experiments. (b) Conditions for the generation of 110 μm-diameter droplets. The combined total flow rate of the agarose solutions was 0.12 mL/h.

These two effects are presented quantitatively in Fig. 3a where the variation in the mean diameter of droplets, D, is plotted as a function of Q_o for the different values of α. The range of the values of Q_o used in the present work was limited by the requirement producing droplets with a targeted diameter of 110 μm. The decrease in D with increasing value of Q_o occurred due to the increasing shear stress imposed by the oil phase on the stream of the mixed agarose solution. Similarly, with increasing α (and hence, with increasing viscosity of the agarose solution) the shear stress imposed on the stream of the droplet phase reduced leading to the generation of larger droplets. The results presented in Fig. 3a indicate that, in order to produce droplets with $D = 110$ μm (shown with a horizontal dashed line), the value of Q_o had to be tuned for the varying concentration of agarose in the droplet phase. Fig. 3b provides guidance for the generation of 110 μm-diameter droplets from agarose solutions at the varying values of α.

Since two parallel laminar streams of liquids with different viscosities may not share the volume of the MF channel in the ratio of their volumetric flow rates [37], we determined the real concentration of agarose, C_{ag}, in the droplet phase by conducting ATR-FTIR experiments as described in Section 2.2.2. Fig. 4a shows the variation in C_{ag} *vs.* α in the mixed droplet phase (Stream 1 + Stream 2) prior to the formation of droplets. For comparison, we plotted the estimated values, calculated as

$$C'_{ag} = [(C_{ag,1}\, Q_{ag,1}) + (C_{ag,2}\, Q_{ag,2})]/(Q_{ag,1} + Q_{ag,2}) \quad (3)$$

where $C_{ag,1}$ and $C_{ag,2}$ are the concentrations of agarose in Streams 1 and 2, respectively, and $Q_{ag,1}$ and $Q_{ag,2}$ are the flow rates of Streams 1 and 2, respectively. The experimentally determined and the estimated concentration profiles showed a similar trend, that is, the increase in agarose concentration at higher values of α, and with identical values of C_{ag}.

Next, we characterized the properties of the agarose solution for $0.5 \le C_{ag} \le 3.0$ wt.% and the temperature of 32 °C (the temperature at the point of emulsification). The value of interfacial tension, γ_{12}, between the continuous phase (a 3 wt.% solution of Span-80 in mineral oil) and agarose solutions at varying C_{ag} was ~2.2 mN/m for the entire range of concentrations of agarose solutions. The variation of viscosity of agarose solution with increasing C_{ag} is presented in Fig. 4b. In the designated range of C_{ag}, the viscosity of the solution increased from 0.5×10^{-2} to 2.4×10^{-1} Pa·s.

Fig. 4c shows the variation in the mean diameter of droplets, D, plotted as a function of the product $Ca_d \times \beta$ where Ca_d is the Capillary number of the droplet phase and $\beta = Q_o/(Q_d + Q_o)$. The value of the Ca_d was calculated as $Ca_d = \mu_d U_d/\gamma_{12}$ where μ_d and U_d are the dynamic viscosity and the velocity of the aqueous agarose solutions, respectively. While for $C_{ag} < 2$ wt.% (md < 0.08 Pa·s)

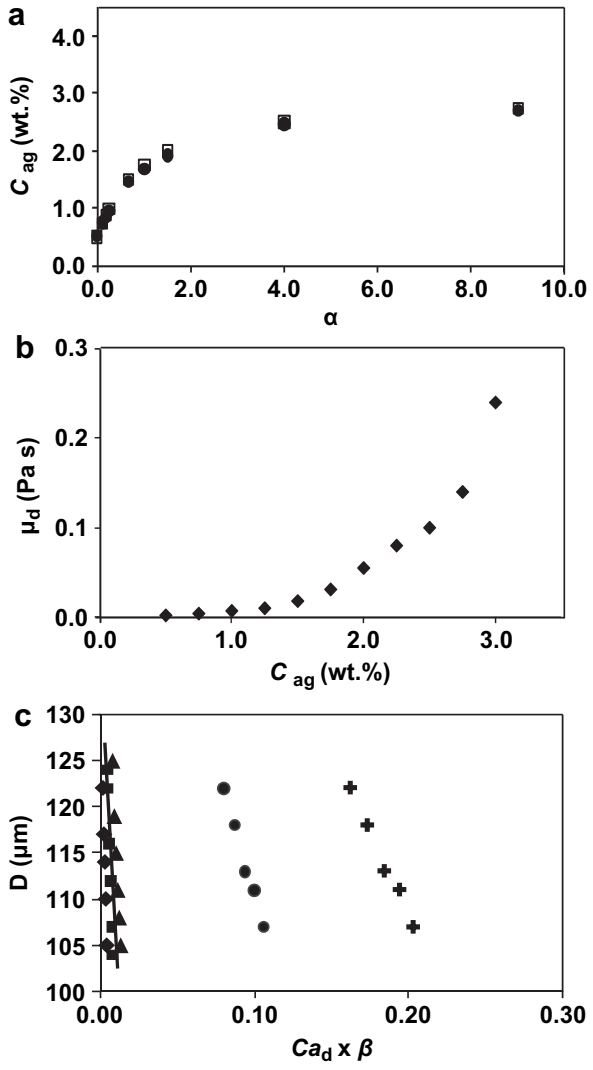

Fig. 4. (a) Variation in experimentally determined (•) and estimated (□) agarose concentration in the droplet phase, plotted as a function of α. Data were acquired from the absorbance of the C–O–C vibrational peak of agarose and converted to concentrations using the Beer–Lambert law. (b) Variation in the viscosity of the droplet phase measured at 32 °C, plotted as a function of C_{ag}. (c) Variation in droplet diameter plotted as a function of the product of the Capillary number of the droplet phase and the ratio $Q_o/(Q_d + Q_o)$ for α of 0.11 (◆), 0.25 (■), 0.67 (▲), 1.50 (•), and 9.00 (+).

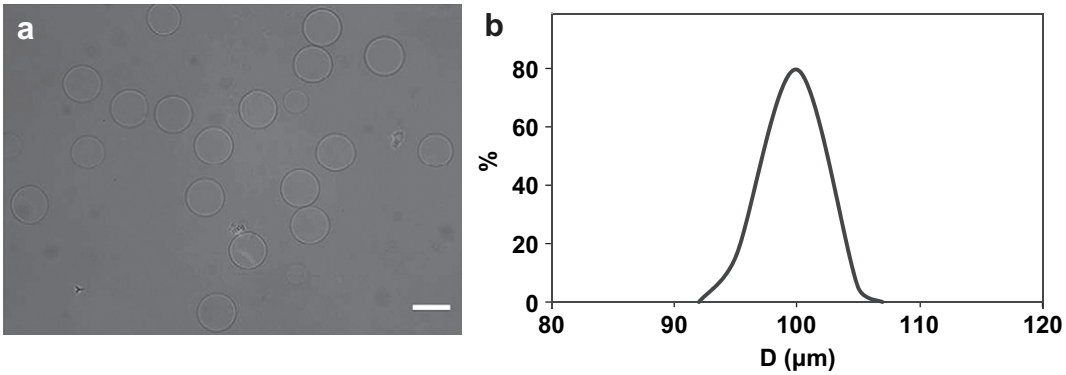

Fig. 5. Optical microscopy images (a) and size distribution (b) of agarose microgels transferred in the PBS buffer. C_{ag} = 2 wt.%. The scale bar is 100 μm.

the relationship D *vs.* $Ca_d \times \beta$ followed the master curve and provided a practical guidance for the generation of droplets with a particular diameter, for higher agarose concentrations it was difficult to find a single model. We note however that in the range of C_{ag} used in the present work, the solutions had Newtonian liquid properties [38].

Fig. 5a shows typical optical microscopy image of agarose microgels derived from precursor droplets and transferred to the PBS buffer. The microgels had a round shape and the average diameter that was approximately equal to the mean diameter of the corresponding droplets. The microgels had a narrow size distribution, as shown in Fig. 5b. The polydispersity (defined as the standard deviation in the dimensions of the droplets divided by the mean diameter) of microgels did not exceed 6%.

In the next step, we examined the mechanical properties of macroscopic agarose gels derived from solutions at $0.75 \leq C_{ag} \leq 3.0$ wt.%. The variation in the elastic shear modulus, G', plotted as a function of agarose concentration, is shown in Fig. 5. The values of G' were determined at 4 °C (the temperature of microgel preparation), room temperature (25 °C), and 37 °C (the temperature of cell culture). With increasing temperature, the gels became weaker. For example, at 4 °C, the value of G' spanned the range from 26 (C_{ag} = 0.75 wt.%) to 4420 Pa (C_{ag} = 3.0 wt.%), while at 37 °C the values of G' varied from ~1 Pa (C_{ag} = 0.75 wt.%) to 700 Pa (C_{ag} = 3.0 wt.%). The decrease in the value of G' at elevated temperatures occurred due to the dissociation of the cross-linked agarose molecules that formed a gel network.

To further mimic cell culture conditions, the gels were transferred into a PBS solution and incubated overnight at 37 °C. Following overnight exposure to the aqueous medium incubation, the concentration of agarose in the gels reduced. For example, for the original gel with C_{ag} = 3 wt.%, the concentration of agarose decreased to $C_{ag,r}$ = 2.76 wt.%. The variation in G' *vs.* $C_{ag,r}$ (calculated using the results shown in Fig. 6a) is shown in Fig. 6b. For the range of C_{ag} used in MF experiments (corresponding to $0.77 \leq C_{ag,r} \leq 2.76$ wt.%) the range of G' was from 15 Pa to ~520 Pa (the gel produced at C_{ag} = 0.75 wt.% was not mechanically stable).

The relatively low values of G' achieved in the present work were presumably caused by the short time that agarose was allowed to gel: typically, agarose gels reach equilibrium values of shear moduli at substantially longer time scales [39]. Thus we expect that longer gelation times will lead to an increase in the rigidity of agarose microbeads, which will be tested using atomic force microscopy [40]. Secondly, the MF strategy can be extended to the emulsification of more concentrated agarose solutions with a higher viscosity [41]. In order to achieve good mixing between the two streams with a large difference in viscosities of the liquids, the design of the MF device may require a modification, e.g., introduction of the third inlet channel supplying a liquid with an intermediate viscosity and/or providing a more 'symmetric' emulsification [42].

In cell encapsulation experiments, we used R1 and YC5–YFP–NEO murine embryonic stem (mES) cells suspended in the droplet phase to a concentration of 8×10^6 cells/mL. The microgels were produced at C_{ag} = 2 wt.%, which corresponded to $G' \approx 200$ Pa after overnight incubation of microgels in PBS buffer at 37 °C. For the precursor droplets with a mean diameter of 110 μm we achieved an encapsulation efficiency of 98.5%. The representative images of R1 and YC5–YFP–NEO mES cells encapsulated in the agarose microgels are shown in Fig. 7a and b, respectively. Following the encapsulation of mES cells in agarose microgels, cell viability was determined to be 79.6 ± 2.5% and 80.0 ± 1.6% for R1 and YC5–YFP–NEO mES cells,

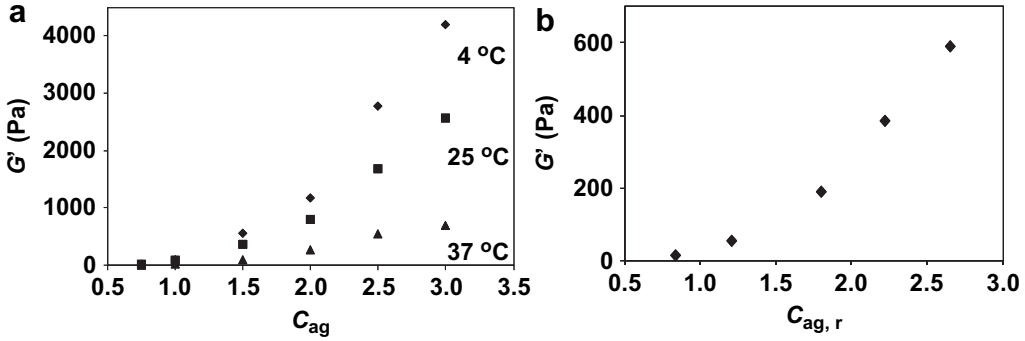

Fig. 6. (a) Variation in the elastic shear modulus, G', of agarose gels with varying concentrations of agarose, C_{ag}, measured at 4 °C (◆), 25 °C (■) and 37 °C (▲). (b) Variation in the value of G' of agarose gels following uptake of water during overnight incubation in the PBS buffer at 37 °C. $C_{ag,r}$ is the concentration of agarose in the gels swollen at 37 °C.

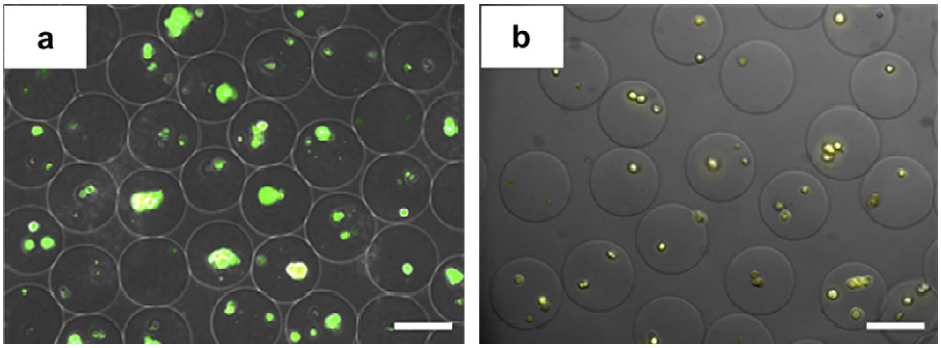

Fig. 7. Fluorescence optical microscopy images of agarose microgels encapsulating (a) R1 and (b) YC5–YFP–NEO mES cells in HBSS buffer. Encapsulation occurred at a total cell concentration of 8×10^6 cells/mL in the droplet phase at $C_{ag} = 2$ wt.%. The scale bar is 100 μm.

respectively. Optical microscopy images were taken and cell viability tests were performed immediately after the transfer of the cell-laden microgels into HBSS buffer.

3. Conclusions

We have demonstrated an MF method for the continuous, fast, high-throughput generation of agarose-based 3D cellular microenvironments with precisely controlled dimensions and varying mechanical properties. The method paves the way for efficient studies of the effect of microenvironment elasticity on the behaviour of cells, which, after incubation within agarose microgels, can be analyzed by optical microscopy and flow cytometry. The method can be extended to the generation of combinatorial of libraries of cellular microenvironments from a large number of biological polymers.

Acknowledgements

The authors thank Canada Research Chair Grant (NSERC Canada) and Canadian Institutes for Health Research (CHIR) for financial support of this work. AK thanks NSERC Canada for NSERC-USRA scholarship. The authors acknowledge assistance in experimental work by Ms. Lsan Tzadu.

Appendix. Supplementary data

Supplementary data associated with this article can be found, in the online version, at doi:10.1016/j.biomaterials.2010.10.033.

Appendix

Figures with essential colour discrimination. Certain figures in this article, particularly Figs. 1, 3 and 7 may be difficult to interpret in black and white. The full colour images can be found in the online version, at doi:10.1016/j.biomaterials.2010.10.033.

References

[1] Leipzig ND, Shoichet MS. The effect of substrate stiffness on adult neural stem cell behaviour. Biomaterials 2009;30:6867–78.
[2] Flanagan LA, Ju YE, Marg B, Osterfield M, Janmey PA. Neurite branching on deformable substrates. Neuroreport 2002;13:2411–5.
[3] Reilly GC, Engler AJ. Intrinsic extracellular matrix properties regulate stem cell differentiation. J Biomech 2010;43:55–62.
[4] Discher DE, Mooney DJ, Zandstra PW. Growth factors, matrices, and forces combine and control stem cells. Science 2009;324:1673–7.
[5] Pelham RJ, Wang YL. Cell locomotion and focal adhesions are regulated by substrate flexibility. Proc Natl Acad Sci U S A 1997;94:13661–5.
[6] Beningo KA, Lo CM, Wang YL. Flexible polyacrylamide substrata for the analysis of mechanical interactions at cell–substratum adhesions. Methods Cell Biol 2002;69:225–39.
[7] Cukierman E, Pankov R, Stevenes DR, Yamada KM. Taking cell–matrix adhesions to the third dimension. Science 2001;294:1708–12.
[8] Engler AJ, Sweeney HL, Sen S, Discher DE. Matrix elasticity directs stem cell lineage specification. Cell 2006;126:677–89.
[9] Blacklock J, Vetter A, Lankenau A, Oupicky D, Möhwald H. Tuning the mechanical properties of bioreducible multilayer films for improved cell adhesion and transfection activity. Biomaterials 2010;31:7167–74.
[10] Kloxin AM, Benton JA, Anseth KS. In situ elasticity modulation with dynamic substrates to direct cell phenotype. Biomaterials 2010;31:1–8.
[11] Pedersen JA, Swartz MA. Mechanobiology in the third dimension. Ann Biomed Eng 2005;33:1469–90.
[12] Temenoff JS, Park H, Jabbari E, Sheffield TL, LeBaron RG, Ambrose CG, et al. In vitro osteogenic differentiation of marrow stromal cells encapsulated in biodegradable hydrogels. J Biomed Mater Res A 2004;70A:235–44.
[13] Batorsky A, Liao JH, Lund AW, Plopper GE, Stegemann JP. Encapsulation of adult human mesenchymal stem cells within collagen-agarose microenvironments. Biotechnol Bioeng 2005;92:492–500.
[14] Dang SM, Gerecht-Nir S, Chen J, Itskovitz-Eldor J, Zandstra PW. Controlled, scalable embryonic stem cell differentiation culture. Stem Cells 2004;22:275–82.
[15] Guvendiren M, Burdick JA. The control of stem cell morphology and differentiation by hydrogel surface wrinkles. Biomaterials 2010;31:6511–8.
[16] Karoubi G, Ormiston ML, Stewart DJ, Courtman DW. Single-cell hydrogel encapsulation for enhanced survival of human marrow stromal cells. Biomaterials 2009;30:5445–55.
[17] Weber LM, Anseth KS. Hydrogel encapsulation environments functionalized with extracellular matrix interactions increase islet insulin secretion. Matrix Biol 2008;27:667–73.
[18] Beebe DJ, Mensing GA, Walker GM. Physics and applications of microfluidics in biology. Annu Rev Biomed Eng 2002;4:261–86.
[19] Clausell-Tormos J, Lieber D, Baret JC, El-Harrak A, Miller OJ, Frenz L, et al. Droplet-based microfluidic platforms for the encapsulation and screening of mammalian cells and multicellular organisms. Chem Biol 2008;15:0427–37.
[20] Brouzes E, Medkova M, Savenelli N, Marran D, Twardowski M, Hutchison JB, et al. Droplet microfluidic technology for single-cell high-throughput screening. Proc Natl Acad Sci U S A 2009;106:14195–200.
[21] Tan WH, Takeuchi S. Monodisperse alginate hydrogel microbeads for cell encapsulation. Adv Mater 2007;19:2696–701.
[22] Shim JU, Olguin LF, Whyte G, Scott D, Babtie A, Abell C. Simultaneous determination of gene expression and enzymatic activity in individual bacterial cells in microdroplet compartments. J Am Chem Soc 2009;131:15251–6.
[23] Huebner A, Srisa-Art M, Holt D, Abell C, Hollfelder F, deMello AJ, et al. Quantitative detection of protein expression in single cells using droplet microfluidics. Chem Commun 2007;12:1218–20.
[24] Huebner A, Olguin LF, Bratton D, Whyte G, Huck WT, deMello AJ, et al. Development of quantitative cell-based enzyme assays in microdroplets. Anal Chem 2008;80:3890–6.
[25] Tumarkin E, Kumacheva E. Microfluidic generation of microgels from synthetic and natural polymers. Chem Soc Rev 2009;38:2161–8.
[26] Baret JC, Miller OJ, Taly V, Ryckelynck M, El-Harrak A, Frenz L, et al. Fluorescence-activated droplet sorting (FADS): efficient microfluidic cell sorting based on enzymatic activity. Lab Chip 2005;9:1850–8.
[27] Hayashi A, Kanzaki T. Swelling of agarose gel and its related changes. Food Hydrocolloid 1987;4:317–25.
[28] Agudelo CA, Teramura Y, Iwata H. Cryopreserved agarose-encapsulated islets as bioartificial pancreas: a feasibility study. Transplantation 2009;87:29–34.
[29] Pelaez D, Huang CY, Cheung HS. Cyclic compression maintains viability and induces chondrogenesis of human mesenchymal stem cells in fibrin gel scaffolds. Stem Cells Dev 2009;18:93–102.
[30] Iwata H, Kobayashi K, Takagi T, Oka T, Yang H, Amemiya H, et al. Feasibility of agarose microbeads with xenogeneic islets as a bioartificial pancreas. J Biomed Mater Res 1994;28:1003–11.
[31] Lahooti S, Sefton MV. Agarose enhances the viability of intraperitoneally implanted microencapsulated L929 fibroblasts. Cell Transplant 2000;9:785–96.

[32] Xia YN, Whitesides GM. Soft lithography. Annu Rev Mater Sci 1998;28:153–84.
[33] Greener J, Abbasi B, Kumacheva E. Attenuated total reflection fourier transform infrared spectroscopy for on-chip monitoring of solute concentrations. Lab Chip 2010;10:1561–6.
[34] Hadjantonakis AK, Nagy A. FACS for the isolation of individual cells from transgenic mice harboring a fluorescent protein reporter. Genesis 2000;27:95–8.
[35] Haight FA. Handbook of the Poisson distribution. New York, USA: Wiley; 1967.
[36] Christopher GF, Anna SL. Microfluidic methods for generating continuous droplet streams. J Phys D Appl Phys 2007;40:R319–36.
[37] Chan KLA, Niu XZ, deMello AJ, Kazarian SG. Rapid prototyping of microfluidic devices for integrating with FT-IR spectroscopic imaging. Lab Chip 2010;10:2170–4.
[38] Fernández E, López D, Mijangos C, Duskova-Smrckova M, Ilavsky M, Dusek K. Rheological and thermal properties of agarose aqueous solutions and hydrogels. J Polym Sci Part B Polym Phys 2007;46:322–8.
[39] Normand V, Lootens DL, Amici E, Plucknett KP, Aymard KP. New insight into agarose gel mechanical properties. Biomacromolecules 2000;1:730–8.
[40] Raz N, Li J, Fiddes L, Tumarkin E, Walker G, Kumacheva E. Microgels with an interpenetrating network structure as a model system for cell studies. Macromolecules 2010;43:7277–81.
[41] Nie Z, Seo M, Xu S, Lewis PC, Mok M, Kumacheva E, et al. Emulsification in a microfluidic flow-focusing device: effect of the viscosities of the liquids. Microfluidics and Nanofluidics 2008;5:585–94.
[42] Ismagilov RF, Lyon AD, Song H, Tice JD. Formation of droplets and mixing in multiphase microfluidics at low values of the Reynolds and the Capillary numbers. Langmuir 2003;19:9127–33.